Electrical oscillations induced by the metal-insulator transition in VO_2

Hyun-Tak Kim,[1,a)] Bong-Jun Kim,[1] Sungyoul Choi,[1] Byung-Gyu Chae,[1] Yong Wook Lee,[1,2,b)] T. Driscoll,[3] M. M. Qazilbash,[3] and D. N. Basov[3]
[1]*Metal-Insulator Transition Laboratory, ETRI, Daejeon 305-350, Republic of Korea*
[2]*School of Electrical Engineering, Pukyong National University, Busan 608-739, Republic of Korea*
[3]*Department of Physics, University of California-San Diego, La Jolla, California 92093, USA*

(Received 25 August 2009; accepted 20 November 2009; published online 21 January 2010)

We systematically investigate the characteristics of an electrical oscillation observed in two-terminal vanadium dioxide (VO_2) devices. These oscillations are observed at room temperature in a simple electrical circuit without inductive components. The circuit is composed only of a dc voltage source, the VO_2 device, and a standard resistor connected in series with the device. We explain why the observed oscillations are a result of the percolative metal-to-insulator transition (MIT) of VO_2 and the coexistence of the metal and insulating phases. Specifically, oscillations are attributed to the construction and destruction of capacitive regions composed of regions of the semiconducting phase, (as dielectric material) and metallic phase electron carriers, induced by the MIT (as capacitor electrodes). Since the coexistence of these phases—and thus the capacitive regions—is destroyed by elevated temperature, the MIT oscillation is not explained in terms of significant heat input but rather in terms of a voltage-triggered effect. It is also discussed whether the current jump at the onset of the oscillations is driven by Mott physics or by Peierls physics relying on a structural phase transition. Furthermore, the electrical parameter space surrounding these oscillations is explored, and a generation window is identified. Within this generation window, the oscillation frequency can be continuously tuned by adjusting applied voltage or by an external circuit component, such as resistor or added capacitor. The frequency of oscillations can be increased up to >1 MHz.
 [doi:10.1063/1.3275575]

I. INTRODUCTION

Mott[1] predicted in 1949 that a first-order discontinuous metal-insulator transition (MIT) could arise from the removal of electrons in a strongly correlated electron system (or Mott insulator). The critical driving parameter in this transition is the on-site repulsive Coulomb interaction U_C.[2] This concept has been derived by the extension of the Brinkman–Rice picture[3,4] and is based on inhomogeneity. The removal of electrons, regarded as doping of hole carriers, causes a breakdown of U_C in a Mott insulator with a hole concentration below 0.01% and induces the breakdown of an energy gap formed by U_C through impact ionization;[5–7] this is the hole-driven MIT generated at a critical hole concentration, n_c, not the metallic minimum carrier density in the Mott criterion.[1,4] In this case, both a metal phase with electron carriers and a semiconductive system with hole carriers can be formed. The metal phase has a strong correlation between electrons.[2,8] The semiconductive system is a remnant component of the parent Mott insulator which is an extrinsic compound semiconductor with disorder, impurities, dislocation, etc. The Mott system (or insulator) has two kinds of carriers[4,9] and is intrinsically inhomogeneous.[10,11]

In strongly correlated system, there are several explanations besides Mott's first-order theory: a Hubbard MIT,[12] which undergoes a continuous transition from metal to insulator following the increase in U, and a Peierls continuous MIT [13] driven by electron-phonon interactions, such as charge density wave (CDW), which induce a structural phase transition (SPT).[14]

In the context of the above MIT theories, VO_2 ($3d^1$) is a very interesting material because it is a representative insulator with both an energy gap of 0.6 eV and the metallic electronic structure of half filling. It undergoes a large resistance change (regarded as the MIT) near critical temperature $T_C \approx 67$ °C and a SPT between the monoclinic structure (below T_C) and the tetragonal rutile structure above T_C.[15]

The insulator structure of VO_2 was known as the monoclinic one, M_1, at enough low temperatures compared to T_C and at room temperature. With increasing temperature, M_1 changed to M_2 just below T_C via an intermediate triclinic monoclinic structure T, and finally was transformed to the rutile R tetragonal structure of the metallic phase above T_C.[16] M_2 is composed of two distorted structures; one-half of the V chain pairs but does not twist (this forms charge ordering of CDW) and the other half twists but does not pair (this is an equally spaced V zigzag chain and forms the Mott–Hubbard insulator.).[17,18] M_1 is defined by a superposition of two distorted structures in M_2.[17,18] For $V_{1-x}Cr_xO_2$, with doping concentration x, the M_1 structure of the insulator phase at room temperature was transformed into M_2 via M_3.[17] Moreover, for VO_2 nanorods with the semiconducting characteristic below and over 190 K, a small jump in conductivity and photocurrent decay near 190 K was interpreted as a first-order SPT between M_2 and T structures.[19]

Researches on the MIT of VO_2 have mainly focused on the mechanism responsible for the SPT between the mono-

[a)]Electronic mail: htkim@etri.re.kr.
[b)]Electronic mail: yongwook@pknu.ac.kr.

clinic insulating phase and the tetragonal rutile metal phase.[20–24] However, Kim *et al.*[5,8] concentrated researches on the presence of a resistivity change as MIT, which is not accompanied by any SPT, and the observation of a strong correlation. The presence of a MIT independent of any SPT (a metal phase with the monoclinic structure) was experimentally observed by several experiments such as Raman scattering with temperature,[25] Raman-scattering under high pressure,[26–28] infrared transmission and reflectivity for $V_{1-x}Cr_xO_2$ under high pressure,[29] careful study of coherent phonons,[30] micro-X-ray diffraction,[31] programmable critical-temperature sensor,[32] strain-induced MIT in single-domain nanobeam,[33] and electron diffraction.[34] Wei *et al.*[33] showed a metal phase in the coexistence regime in nanobeams below a temperature where a kink occurs between the supercooled and stable metallic phases. Since the kink is similar to a kink of the SPT measured at *I-V* curves,[31] the kink can be regarded as the SPT. Then the metallic phase below the kink temperature can be interpreted as the metal phase with a monoclinic structure. Moreover, the metal phase with a monoclinic structure for a $V_{1-x}Mo_xO_2$ ceramic sample was also observed by a nanolevel x-ray diffraction experiment.[35] Gopalakrishnan *et al.*[36] revealed that MIT is independent of the SPT through simulations based on the thermal model. The divergent effective mass in the metal phase as evidence of strong correlations was analyzed via using effective medium theory to determine optical parameters within true nanoscale grain regions in a heterogeneous system.[8] Hole charges below $T_C \approx 67$ °C were observed by Hall effect measurement.[5,9] The electrostatic method also revealed the presence of hole charges in VO_2.[37] The Mott–Hubbard bands were directly observed by resonance of $3d^0+3d^1L$ and $3d^1$C states by V $2p$-$3d$ resonant photoemission spectroscopy[38] and broadness of π band including d_{11} band.[39]

The summation of the above investigations is overwhelming evidence supporting a hole-driven Mott MIT. However, the issue is yet to be completely settled, due to some evidence in favor of Peierls MIT, such as observation of the tetragonal phonon at 6 THz[40] and a rapid decrease in transmission[41] observed by the femtosecond technique. Thus, it has been long debated whether this MIT in VO_2 is driven by Mott or Peierls physics.[18,42]

The voltage-induced current jump observed in experiments,[5,43] regarded as the MIT, is not generated by temperature increase and thus is evidence for a hole-driven MIT. This electrical jump has attracted interest of great many researchers because an abrupt resistance switching mediated by voltage-induced MIT can give versatile practical applications.[5,43]

The diverging MIT instabilities[3,4] for a strongly correlated system could predict such an electrical oscillation in a serial circuit composed of a resistance and a MIT device.[44] Observations of the MIT electrical oscillation in VO_2 were previously reported.[45,46] This oscillation generated by the voltage-induced MIT can be evidence to support the hole-driven Mott MIT model because such high-frequency oscillations are unlikely to exist within a thermally driven SPT Peierls system. The thermal timescales, as well as the known hysteretic behavior of the SPT when switching between monoclinic and tetragonal structures occurs, prohibit such high-frequency oscillations.

In earlier studies, electrical oscillations similar to those we observed, but with a sinusoidal waveform, were observed in GaAs,[47] $K_{0.3}MoO_3$,[48] and θ-(BEDT-TTF)$_2$CsCo(SCN)$_4$.[49,50] The Gunn oscillation in GaAs was explained in terms of the negative differential resistance (NDR) caused by mobility change from (100) to (110).[51] The NDR characteristic is similar to the thyristor one.[52] For $K_{0.3}MoO_3$, the sliding motion of the CDW undergoing the SPT was suggested as the oscillation mechanism, and the oscillation frequency f_{osc} could be changed from 10 to 17 kHz by varying the applied voltage at 17 K.[48] The 40 Hz oscillation in θ-(BEDT-TTF)$_2$CsCo(SCN)$_4$ was also observed at 4.2 K.[49] The current jump in the organic material was explained by melting of charge ordering with a charge difference between nearest neighbors. The charge difference is regarded as the CDW. The melting of the charge ordering is similar to the sliding of the CDW in $K_{0.3}MoO_3$ and indicates the melting of the structure distorted by electron-phonon interaction. This analysis is acceptable for organic and CDW materials. However, as far as a correlated material such as VO_2, the mechanism of the oscillation is different from that in CDW materials. The physical reasons for these differences will be discussed in Sec. IV.

In this paper, we investigate the characteristics of a high-frequency room-temperature electrical oscillation observed in the VO_2-based two-terminal devices with S-type NDR characteristics. We demonstrate the generation mechanism of this oscillation by analyzing experimental data based on inhomogeneity. We show that increasing applied source voltage to the device causes percolation and increases the oscillation frequency f_{osc} by effectively decreasing the device capacitance.

Values for the capacitance of the device are found by fitting exponential charging curves. Furthermore, an overall generation window for the MIT oscillation is found in terms of the external resistance and source voltage. In particular, the effect of the external circuit components, such as a voltage source, resistor, and capacitor, on f_{osc} is systematically investigated. Thus, we reveal that f_{osc} can be designed to be increased up to >1 MHz and controlled by simple adjustment of some external circuit components.

II. EXPERIMENTS

In order to fabricate the two-terminal VO_2 device shown in Fig. 1(a), VO_2 thin films were grown on sapphire (Al_2O_3) substrates by employing a sol-gel method.[53] Note that VO_2 films could be deposited by several deposition methods.[54] The films were patterned into a line shape to make a current channel with photolithography processes and a rf ion-beam milling technique. A Ni electrode layer was deposited on the etched VO_2 layer using a rf magnetron sputter deposition

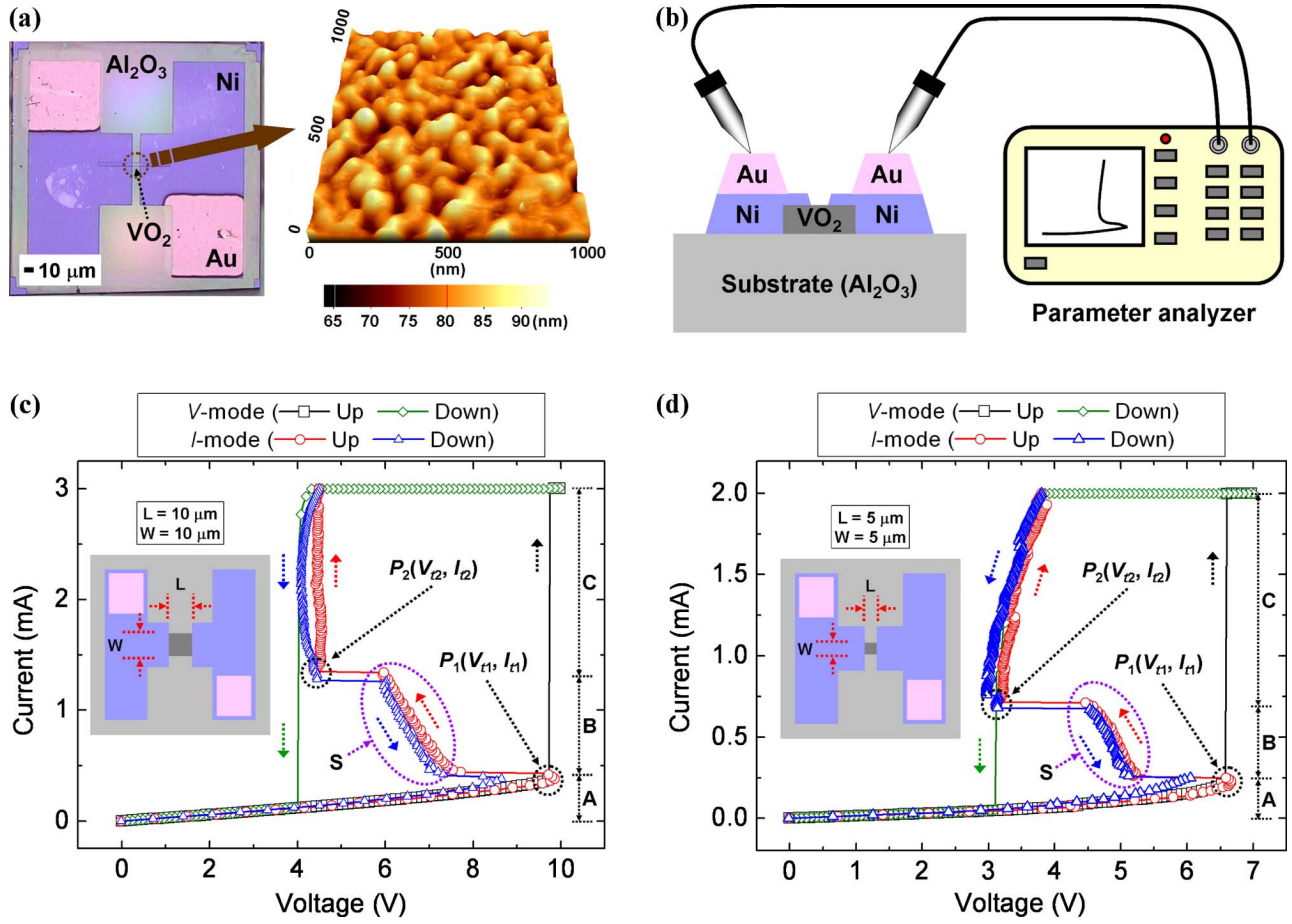

FIG. 1. (Color online) (a) Optical microscope plane-view image of a VO_2-based two-terminal device and the surface morphology of the VO_2 film used in the device. (b) Schematic diagram of the experimental setup to measure *I-V* characteristics of the device. Measured *I-V* hysteresis characteristics of (c) device I (10×10 μm^2) and (d) device II (5×5 μm^2).

technique and was patterned with a lift-off method. For direct microcontact electrical measurements, square-shape gold electrodes of 50×50 μm^2 were patterned on Ni electrodes of the device. The width of the VO_2 patch was designed to be narrower than that of the electrodes to avoid any delayed transition of VO_2 outside the electrodes. The final dimensions of the exposed film patches in the fabricated devices were 10×10 μm^2 (device I) and 5×5 μm^2 (device II). The thickness of the VO_2 films was approximately 100 nm.

The schematic diagram of the experimental setup to measure *I-V* characteristics of the device is shown in Fig. 1(b). For the *I-V* measurements, we used a microprobe station (Micromanipulator) with tungsten probes (5 μm in diameter) and a parameter analyzer (Agilent B1500A). The Ohmic contact resistance of the devices was below 1 Ω, which is negligible compared with the device resistance R_D at room temperature. The *I-V* characteristics of the devices were obtained by using the *V*-mode and *I*-mode of the parameter analyzer. The *V*-mode and *I*-mode are the measurement modes to detect the current and voltage across the device, I_D and V_D, as a function of the applied voltage (*V*-mode) and current (*I*-mode), respectively. Moreover, the stability of the MIT current-jump threshold point, responsible for the observed switching, was confirmed.[55]

III. MEASUREMENT OF MIT ELECTRICAL OSCILLATION

A. Oscillation measurement and investigation of its generation mechanism

Figure 1(a) shows an optical microscope plane-view image of the fabricated two-terminal VO_2 device (device I) and the surface morphology of the VO_2 film used in the device (a rms roughness of ~5 nm). The film surface was comprised of grains of several different sizes. At room temperature, the VO_2 film has almost insulating VO_2 grains (high resistance dielectric components). At a critical temperature (~340 K), high resistance insulating grains begin to turn into low resistance metallic ones, and most insulating grains have transitioned into metallic ones just after the critical temperature.[27,28] Any void between grains (which will have large resistance) and non-VO_2 phases in the film such as V_2O_5 can affect R_D throughout the entire process of the voltage-induced MIT.[23] Recently, it was observed that the MIT begins percolation near grain boundaries or void regions, suggesting that these have a strong role in the MIT transition dynamics.[11]

Figures 1(c) and 1(d) show the *I-V* hysteresis loops measured at room temperature for device I and device II, respectively. Below the threshold of any current-jumps [in region A of Figs. 1(c) and 1(d)], device I and device II exhibit semi-

conducting behavior with hole charges.[4,9] There exist two threshold instability voltages (V_{t1}, V_{t2}) where abrupt current changes happen. At V_{t1}, a critical carrier density inducing the jump, n_c, is reached.[4] In *V*-mode traces, $(V_{t1} \approx 9.7\ \text{V},\ V_{t2} \approx 4.0\ \text{V})$ in device I and (6.6 V, 3.1 V) in device II were measured. The currents at V_{t1} and V_{t2} are designated as I_{t1} and I_{t2}, respectively. The *V*-mode traces have large hysteresis loops with black and green jumps corresponding to negative and positive jumps in resistance, respectively. In the *I*-mode traces of both Figs. 1(c) and 1(d), a typical feature of the S-type NDR is shown between instability $P_1(V_{t1}, I_{t1})$ and instability $P_2(V_{t2}, I_{t2})$. The NDR behavior arises from the restriction of current and has little hysteresis width. This indicates that *I*-mode generates little heat and no SPT. Anomalous behavior—decreasing voltage with increasing current—was observed in a semiconductor phase between instabilities P_1 and P_2 (S section in region B). This behavior indicates that the MIT occurs gradually, resulting in a gradual decrease in resistance (gradual increase in electrical conductivity). This observation is interpreted as evidence for a percolative transition[8,28,56] and is evidence of inhomogeneity in the VO_2 film. It is also observed by comparing device I with device II that the increase in the device dimension causes both threshold voltages and corresponding currents to increase and thus the NDR region to expand as well. Despite the dimension change, however, no noticeable variation was observed in the differential resistance (dV/dI), estimated as approximately $-500\ \Omega$ from the measurement results. Furthermore, the oscillation is affected by external parameters such as a kind of electrodes, lattice-film mismatch, and film thickness. When electrical characteristics of a device are changed by the external parameters, current near zero voltage (leakage current), V_{t1}, and I_{t2} vary,[5] for example, a large contact resistance between film and a metal electrode with a low conductivity, a large lattice-substrate mismatch, and a more thick film induce a large leakage current, a reduced V_{t1}, and an increased I_{t2}.

Moving on to the experiments involving electrical oscillation, Fig. 2(a) shows a schematic diagram of the electrical circuit used for generating the MIT oscillation and controlling f_{osc}. The single-loop circuit was composed of a VO_2 device (device I or device II), a voltage source of a dc voltage V_S, and an external resistor of a resistance R_E. In order to reduce the generation of an excess Joule heat, both a function generator (Agilent 33120A) and a dc power supply were used for generating rectangular voltage pulses with a variety of dc offsets. The oscillatory electrical responses were recorded by a digital oscilloscope (HP 54810A). An external capacitor of a capacitance C_E in the dashed box can also be connected in parallel to the external resistor giving further control of f_{osc}. In fact, all circuit parameters (V_S, R_E, and C_E) can act as frequency tuning controls, and related experimental results are provided in Figs. 4 and 5.

Figure 2(b) shows the oscillatory electrical traces of V_D (blue diamonds) and I_D (red circles) measured with device I at room temperature, when a single voltage pulse with a peak value of V_S (V_S^p) of 13.8 V (including a dc offset of 10 V) and a pulse width of 25 μs is applied (R_E=8 kΩ). The voltage across the external resistor V_E is directly measured, and V_D and I_D are obtained by $(V_S - V_E)$ and (V_E/R_E), respectively. The peak-to-peak amplitudes of the oscillation waveforms of V_D and I_D were measured as ~5.7 V and ~0.7 mA, respectively. The fundamental component of f_{osc} was measured as ~0.525 MHz. Note that a device without the NDR shown in region B of Figs. 1(c) and 1(d) did not generate any oscillation.

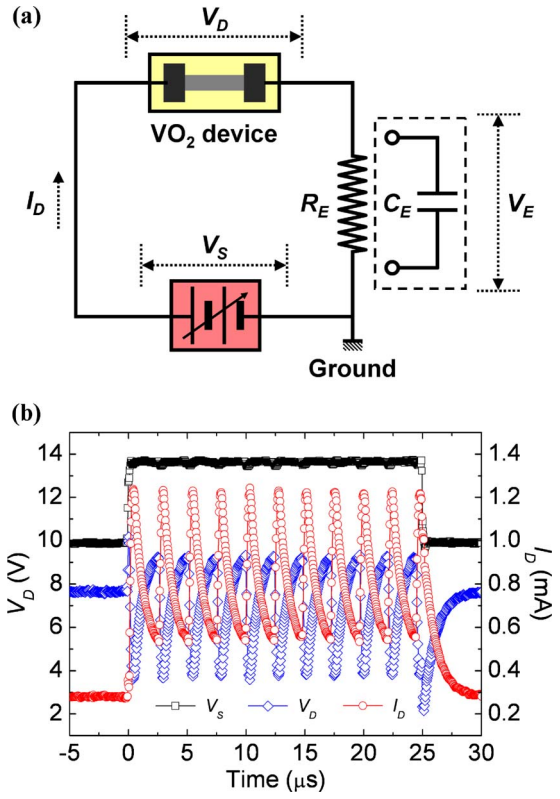

FIG. 2. (Color online) (a) Schematic diagram of the electrical circuit used for the generation of the MIT electrical oscillation. In order to control f_{osc}, an external capacitor in a dashed box can be employed and connected to an external resistor in parallel. (b) Electrical waveforms of V_D (blue diamonds) and I_D (red circles) measured at room temperature when a voltage pulse with V_S^p=13.8 V (including a dc offset of 10 V) and a pulse width of 25 μs are applied (R_E=8 kΩ).

Considering one period of the oscillation in Fig. 2(b), the exponential buildup and decay of V_D and I_D, respectively, are driven by the carrier charging process in a series *RC* circuit—whose electrical response time is restricted by a capacitive time constant τ_0 given by $R_E C_D$ where C_D is a device capacitance. Within one period of the oscillation, the charging curve responses of V_D and I_D, before the MIT threshold jump is triggered, can be fitted by the following expressions derived based on the *RC* circuit analysis;

$$V_D(t) \propto V_S^p[1 - \exp(-t/\tau_0)], \tag{1}$$

$$I_D(t) \propto V_S^p[1 + (R_D/R_E)\exp(-t/\tau_0)]. \tag{2}$$

The overall picture of the oscillations can be understood as follows: in region A of Figs. 1(c) and 1(d), insulating VO_2 grains (high resistance dielectric components with hole charges) constitute most of the VO_2 film. At $V_D = V_{t1}$, an abrupt current jump (MIT) occurs, and an abrupt decrease in R_D takes place. Here insulating grains begin to turn into me-

tallic ones, and metallic electron carriers appear (region B); a capacitor is formed, which consists of a dielectric semiconducting component (S in region B) and the electron carriers. In conjunction with the swift decrease in R_D, V_D instantaneously drops down below V_{t2}, and I_D rapidly increases. Then, V_D is restored to V_{t2} by some repulsive force—designated as the elastic restoring force by Sakai.[46] Behavior of V_D after this moment is determined by I_D affected directly by R_D and R_E.

When we select an appropriate R_E that forces $I_D < I_{t2}$, the device can return to its insulating state. The cycle can repeat with V_D increasing again. In this condition, the temporal buildup of V_D [Eq. (1)] proceeds to occur until V_D reaches V_{t1}. After V_D reaches V_{t1}, the MIT jump occurs, rapidly discharging V_D, and the same process described above repeats as long as V_S^p is large enough to make V_D become V_{t1}. In this manner, the MIT oscillation is maintained between both instabilities $P_1(V_{t1}, I_{t1})$ and $P_2(V_{t2}, I_{t2})$, as indicated in Figs. 1(c) and 1(d).

In the case of R_E selected such that $I_D > I_{t2}$, just after the MIT [region C of Figs. 1(c) and 1(d)], most insulating VO_2 grains have become metallic ones, and the film has few dielectric regions. The decreased dielectric (capacitive) component of the film causes a reduced number of charges to build on the VO_2 device and prevents V_D from increasing to V_{t1} again. In other words, the disappearance of the capacitive component of the film makes it impossible for the VO_2 device to recover its insulating state (high resistance state) and perform oscillations.

B. Nanoscale percolation: Explanation of forming capacitor

An explanation on the presence and absence of the capacitive component in the VO_2 device after the MIT ($V_D > V_{t1}$) is now given, as shown in Fig. 3(a). A VO_2 film composed of many grains [Fig. 1(a)] can be thought of as being comprised of two components: any VO_2 phase (green or red grains) and any non-VO_2 material such as vacuum or V_2O_5 (gray bottom). The amount of the non-VO_2 phase may be negligible in a high-quality film. Looking only at the VO_2 material, when $V_D < V_{t1}$ [plot I of Fig. 3(a)], the film is fully filled with green grains (insulating state) without red grains (metallic state). When V_D starts to exceed V_{t1} [plot II of Fig. 3(a)], one part of the VO_2 phase turns into a metallic state, and the other part still remains an insulating state due to the minute compositional inhomogeneity between VO_2 grains. Green and red grains may act as dielectric components and metal electrodes, respectively. Averaged across the entire film, they build a capacitor across the device. This intermediate state corresponds to the region B in Figs. 1(c) and 1(d). When I_D exceeds I_{t2}, the film is occupied with primarily red grains resulting in vanishing capacitive component of the device [plot III of Fig. 3(a)].

This simple explanation is supported by midinfrared near-field images.[8] Figure 3(b) shows the images of the near-field scattering amplitude over the same 4×4 μm^2 area obtained by using a scattering scanning near-field infrared microscope operating at the infrared frequency of 930 cm^{-1}.[8]

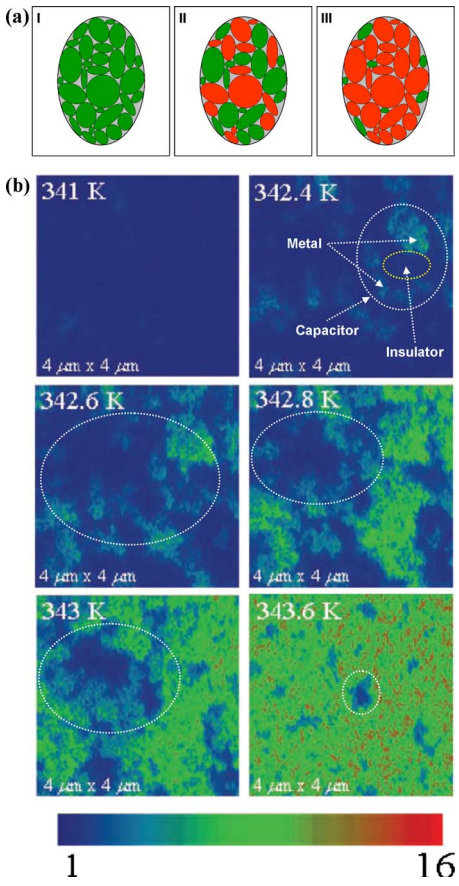

FIG. 3. (Color online) (a) An explanation on the formation of capacitance within the VO_2 device during the MIT. The green and red grains indicate the high and low resistance states (insulating and metallic states) of the VO_2 phase, respectively. The gray bottom is a non-VO_2 phaselike grain boundary. (b) Images of the near-field scattering amplitude over the same 4×4 μm^2 area obtained by using a scattering scanning near-field infrared microscope operating at the infrared frequency $\omega = 930$ cm^{-1}.

These images are displayed for representative temperatures (341.0, 342.4, 342.6, 342.8, 343.0, and 343.6 K) in the MIT regime of VO_2 and show the percolative nature of the MIT in progress. The metallic regions (green and red colors) give higher scattering near-field amplitude compared with the insulating phase (dark blue color), e.g., the region surrounded by the yellow dotted line in Fig. 3(b). These images directly show that the insulating and metallic phases coexist in VO_2 over a finite temperature range in the transition region. Thus, insulating and metallic phases in the region surrounded by the white dotted lines in Fig. 3(b) may act as dielectric components and metal electrodes, respectively, resulting in the formation of a capacitor across the device. Further experimental evidence for the construction and destruction of capacitance in VO_2 comes from observing the infrared resonance frequency of a hybrid-metamaterial comprised of split-ring-resonators and VO_2.[57]

C. Applied voltage dependence of f_{osc}

In order to investigate the dependence of f_{osc} on applied voltage (for a fixed value of R_E with 1 kΩ step), the electrical responses of V_D and I_D were measured for increasing V_S^p. Among the measurement results, Figs. 4(a) and 4(b) show

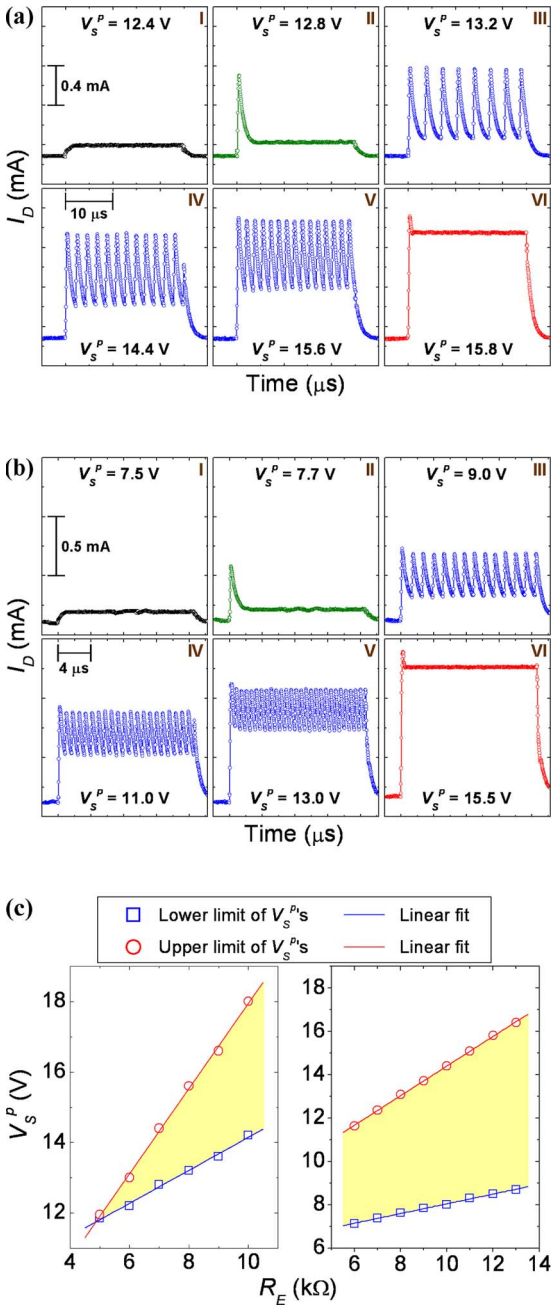

FIG. 4. (Color online) Life cycle of the MIT oscillation of I_D in (a) device I and (b) device II measured at R_E of 8 and 10 kΩ with respect to various values of V_S^p, respectively. (c) A generation window of the MIT oscillation. The lower and upper limits of V_S^p where the oscillation can be generated at each R_E are plotted with blue squares and red circles, respectively. The left and right subplots indicate the generation window of the MIT oscillation in device I and device II, respectively.

the life cycles of the MIT oscillation, measured in I_D, for device I and device II (measured at R_E of 8 and 10 kΩ with respect to various values of V_S^p). In device I and device II, V_S^p's in subplots I, II, III, IV, V, and VI correspond to 12.4, 12.8, 13.2, 14.4, 15.6, and 15.8 V and 7.5, 7.7, 9.0, 11.0, 13.0, and 15.5 V, respectively.

In plot I of Figs. 4(a) and 4(b), current pulses with peak values of ~0.40 and ~0.19 mA and pulse widths of 25 and ~16.67 μs are observed without any I_D oscillation. This implies that V_D does not reach V_{t1} yet. In plot II of Figs. 4(a) and 4(b), current pulses with impulsive peaks whose values are ~1.10 and ~0.58 mA are observed, respectively, and the I_D oscillation is not yet observed. This is because V_S^p is not large enough to make V_D decreased after the MIT reach V_{t1}. In plots III, IV, and V of Figs. 4(a) and 4(b), periodical waveforms composed of impulsive peaks of I_D are observed, i.e., the I_D oscillation is observed. This suggests that V_S^p is large enough to make V_D decreased after the MIT reach V_{t1}. In these three plots (III, IV, and V), we observe that f_{osc} increases in proportion to V_S^p, and a detailed discussion on the relationship between f_{osc} and V_S^p will be provided in Sec. III D. In plot VI of Figs. 4(a) and 4(b), rectangular pulses with average values of ~1.35 and ~1.26 mA, respectively, emerge without the periodical waveform. This extinction of the MIT oscillation is caused by the collapse of the capacitive component of the device [disappearance of dark blue region in Fig. 3(b)] due to Joule heat generated by a large value of I_D induced by V_S^p increase.

In order to find a region of R_E and V_S within which the MIT oscillation can be generated, the oscillation characteristics of the VO_2 devices were measured with several values of R_E and V_S^p. A specific region of R_E and V_S^p, where the MIT oscillation is generated, can be determined in a two-dimensional domain defined with R_E and V_S^p, as shown in Fig. 4(c). The left and right subplots in Fig. 4(c) indicate the generation window of the MIT oscillation in device I and device II, respectively. The lower and upper limits of V_S^p where the MIT oscillation can be generated for each R_E are plotted with blue squares and red circles, respectively. The solid lines are linear fits of the lower and upper limits of V_S^p, and the yellow region enclosed by solid lines thus illustrates the generation window of the MIT oscillation for our two devices. This oscillation window can also be predicted from both relationships: $V_D \geq V_{t1}$ and $I_D \leq I_{t2}$. The graphical intersection of these two one-dimensional inequalities with two variables (R_E and V_S^p) creates a unique region in the two-dimensional domain of R_E and V_S^p. It can be verified from simple graphical analysis that this calculated region is in good agreement with the measured oscillation window [yellow region of Fig. 4(c)].

D. Analysis of oscillation waveform

In order to further investigate the dependence of f_{osc} on V_S, oscillation waveforms of V_D, measured at R_E=8 kΩ for three values of V_S^p (13.8, 14.6, and 15.4 V), were superimposed, as shown in Fig. 5(a). As mentioned earlier, abrupt drops of V_D from points A, C, and E to points B, D, and F labeled in the figure are induced by the MIT of the VO_2 film. As seen from the figure, we can recognize two important features: the temporal intervals of traces A-B, C-D, and E-F labeled in the figure are nearly the same (~0.36 μs) regardless of V_S^p. The time required for dropped V_D to recover to V_{t2} (by some elastic restoring force[27]) is also nearly the same (~0.14 μs) regardless of V_S^p with respect to each trace B-B′, D-D′, and F-F′. Thus, the time consumed on the exponential growth of V_D from V_{t2} to V_{t1}, e.g., t_1 at V_S^p=15.4 V (or t_2 and t_3 at V_S^p=14.6 and 13.8 V, respectively), dominantly contrib-

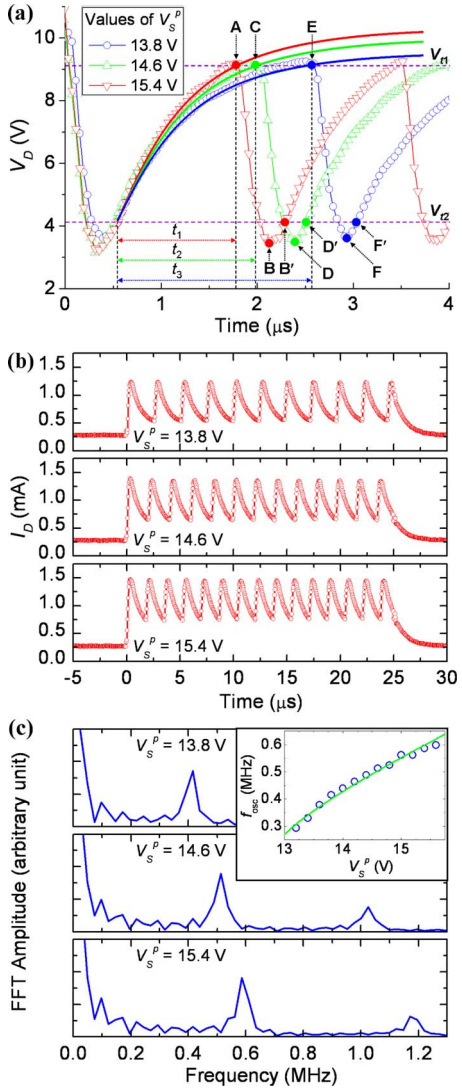

FIG. 5. (Color online) (a) Superimposed waveforms of V_D measured in device I serially connected with R_E=8 kΩ with respect to three values of V_S^p (13.8, 14.6, and 15.4 V). (b) Measured waveforms of I_D oscillation. (c) Their FFT amplitude spectra with respect to various values of V_S^p (only three cases including 13.8, 14.6, and 15.4 V are displayed) at R_E=8 kΩ, when the rectangular voltage pulse with a pulse width of 25 μs is applied to device I. The inset plot shows the functional relationship between f_{osc} and V_S^p.

utes to the determination of f_{osc}. We can fit this exponential growth section from V_{t2} to V_{t1} with the function

$$V_D(t) = (V_A - V_{t2})\{1 - \exp[-(t - t_0)/\tau_0]\} + V_{t2}. \quad (3)$$

This exponential buildup of V_D in Eq. (3) means the buildup of charge on the capacitor in a series RC circuit, which is predicted in Eq. (1). This means that τ_0 in Eq. (3) limiting the maximum f_{osc} is the same as that in Eq. (1), and τ_0 is proportional to $C_D R_E$. τ_0's of the fitting curves evaluated from the traces were ~0.840, ~0.801, and ~0.765 μs for V_S^p's of 13.8, 14.6, and 15.4 V, respectively. This indicates that τ_0 decreases when V_S^p increases, i.e., C_D decreases with the increase in V_S^p. When the effect of R_D dependent on V_S^p on τ_0 is ignored, C_D can easily be estimated as ~105.0, ~100.1, and ~95.6 pF (for V_S^p's of 13.8, 14.6, and 15.4 V, respectively). When we postulate the circuit model of the VO_2 device as the parallel connection of C_D and R_D, τ_0 is given as $R_E C_D[R_D/(R_D+R_E)]$, and thus C_D becomes larger in general cases compared with the above values (~105.0, ~100.1, and ~95.6 pF) and goes to the minimum in a special case such as $R_D \to \infty$, which is the same situation as the above case that τ_0 is independent of R_D. In addition to the relationship between τ_0 and V_S^p, the asymptotic voltage V_A in Eq. (3) also increases with V_S^p. As V_S^p increases, therefore, the exponential curve of V_D in Eq. (3) will be expanded due to the increase in V_A, as shown in red, green, and blue solid lines of Fig. 5(a). This will give rise to a faster arrival of V_D at V_{t1}, resulting in higher f_{osc}.

Figures 5(b) and 5(c) show the waveforms of I_D oscillation and their fast Fourier transform (FFT) amplitude spectra measured with respect to various V_S^p's at R_E=8 kΩ (only three cases including V_S^p's of 13.8, 14.6, and 15.4 V are displayed), respectively, when the rectangular voltage pulse is applied to device I with a pulse width of 25 μs. The inset plot in Fig. 5(c) shows the functional relationship between f_{osc} and V_S^p, and the blue circles indicate the measured values of f_{osc} with respect to the various values of V_S^p. The green solid line indicates the curve fitted by a logarithmic function determining f_{osc} with respect to V_S^p, which is obtained by manipulating Eq. (3) in consideration of the oscillation period. It is observed that the curve initially shows a logarithmic response but asymptotically shows a linear response after V_S^p exceeds 14 V. In an approximately linear region, the tuning sensitivity, defined as $(\Delta f_{osc}/\Delta V_S^p)$, was calculated as 99.18 kHz/V. These results suggest that the VO_2 device can be utilized as a voltage-controlled oscillator, which consists of only two circuit components and is operated by only one voltage source.

E. Effect of external parameters

We now consider controlling f_{osc} using passive external circuit components. f_{osc} is determined by $1/(T_0+T_1)$, where T_0 and T_1 indicate the time required for V_D to increase from V_{t2} to V_{t1} and required for V_D to drop from V_{t1} to V_{t2}, respectively. f_{osc} is mainly dependent on $T_0 = \tau_0 \ln(1+[V_{t1} - V_{t2}]/[V_A - V_{t1}])$, which is obtained by Eq. (3), because T_1 is nearly the same (~0.50 μs) regardless of V_S^p. T_0 depends not only on V_S^p but also on τ_0. This means that f_{osc} can be tuned by varying an external circuit parameter such as R_E. Also, when an external capacitor of a capacitance C_E is connected in parallel with the external resistor, as shown in the dashed box of Fig. 2(a), it becomes another f_{osc} tuning parameter because τ_0 is proportional to $(C_E+C_D)R_E$.

Based on the above discussion, external control of f_{osc} was demonstrated through the adjustment of R_E without external capacitor and the adjustment of C_E with R_E fixed (10 kΩ). This experiment was done in device II, which was especially designed to obtain an enhanced frequency response. This frequency improvement is achieved because the reduced dimension of the VO_2 patch in device II reduces $(V_{t1} - V_{t2})$, but with C_D maintained as nearly the same value as that of device I. Thus, T_0 and f_{osc} in device II become smaller and larger compared with those in device I, respectively.

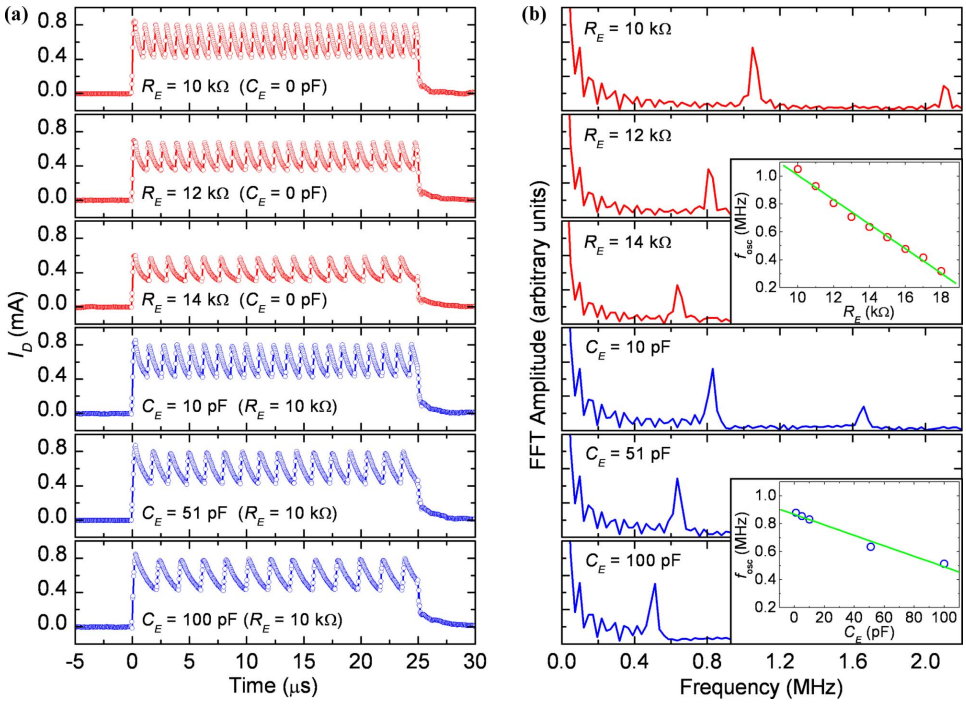

FIG. 6. (Color online) (a) Measured waveforms of I_D oscillation with respect to various external resistances (only three cases including R_E's of 10, 12, and 14 kΩ at C_E=0 are displayed) and various external capacitances (only three cases including C_E's of 10, 51, and 100 pF at R_E=10 kΩ are displayed), when the rectangular voltage pulse is applied to device II with V_S^p of 10 V (no dc offset) and a pulse width of 25 μs. (b) FFT amplitude spectra of I_D oscillation, as shown in Fig. 5(a), measured with respect to various external resistances and capacitances. The upper and lower inset plots show the linearity of the measured values of f_{osc} with respect to R_E and C_E, respectively.

Figure 6(a) shows the measured waveforms of the I_D oscillation with respect to various external resistances (three cases R_E=10, 12, and 14 kΩ at C_E=0 are displayed) and various external capacitances (three cases C_E=10, 51, and 100 pF at R_E=10 kΩ are displayed). As before, a rectangular voltage pulse is applied with V_S^p of 10 V (no dc offset) and a pulse width of 25 μs. Figure 6(b) shows the FFT amplitude spectra of the corresponding I_D oscillation shown in Fig. 6(a).

From the figure, it is clearly observed that f_{osc} decreases with increasing R_E and C_E. A remarkable difference is that the mean value of the peak current and peak-to-peak amplitude have relatively strong dependence on R_E compared with that on C_E. This is caused by the fact that the amplitude of I_D includes a term of $(V_S R_D/R_E)$ directly affected by R_E. The upper and lower inset plots of Fig. 6(b) show the linearity of the measured values of f_{osc} with respect to R_E and C_E, respectively. In each inset, the circular points indicate the measured values of f_{osc} with respect to R_E or C_E, and the solid lines indicate their linear fits. The tuning sensitivities, defined as $(\Delta f_{osc}/\Delta R_E)$ and $(\Delta f_{osc}/\Delta C_E)$, were calculated as 87.89 kHz/kΩ and 3.76 kHz/pF, respectively. The standard deviations of the linear fits in upper and lower insets were calculated as 0.0267 and 0.0282, respectively. These results suggest that a VO_2 two-terminal device can be incorporated as a simple oscillator whose frequency is tuned by only passive circuit components such as resistors and capacitors. In addition, the sensitivity of f_{osc} on V_S^p makes this device a good candidate for a voltage-controlled oscillator. Previous experimental evidence that light can photoinduce the MIT transition in VO_2 suggests that this is another possible external control parameter for these oscillations.

IV. COMPARISION ANALYSIS OF MOTT MIT AND PEIERLS (CDW) MIT

A. The Mott MIT as evidenced by the observed current jump

The observed MIT-driven electrical oscillation occurs between instabilities $P_1(V_{t1}, I_{t1})$ and $P_2(V_{t2}, I_{t2})$ at the *I*-mode trace, and begins at P_1 in Figs. 1(c) and 1(d). Since *I*-mode limits a current flow, the jump appears as a jump in voltage instead of a current jump. This jump has a very small hysteresis, as shown in Figs. 1(c) and 1(d). The small hysteresis indicates that the generated heat is small and does not reach the temperature needed to induce a SPT. This was directly proved by simultaneous measurements of micro-x-ray diffraction and *I-V* measurements.[31] The current jump in the *V*-mode trace in Figs. 1(c) and 1(d), viewed as the MIT, is thus independent of any SPT.[32] A jump in resistance not accompanied by a SPT was also revealed by observing the temperature dependence of coherent phonons[30] and the pressure dependence of phonons.[26–28] It was also disclosed that current jump near the SPT temperature disappears.[5,35] Hole carriers were observed at the semiconductor side near 67 °C.[5,9]

As shown in plot VI's of Figs. 4(a) and 4(b), heat generation caused by an increase in current through our device makes the MIT-driven electrical oscillation disappear. The available experimental results thus draw a decision that the electrical oscillation does not occur above a certain high temperature. It is deduced that this oscillation is below 77 °C[30] based on the experimental results.[5,26–28,30–32] Thus, the microscopic physics responsible for inducing the observed electrical oscillation is that of the hole-driven Mott MIT.[1,3,4]

B. The MIT analysis in view of CDW

Since it has been suggested that the MIT oscillation is related to CDW or charge ordering for $K_{0.3}MoO_3$ and an organic material,[48,49] we discuss the MIT in view of the CDW. CDW (or charge ordering) is a charge imbalance between nearest-neighbor sites. In order to understand charge ordering of CDW, we introduce the Holstein CDW potential energy in the context of the Peierls MIT.[13] The CDW energy is given by $V_{\mathrm{CDW}}=-(b^2/k)(q_i-q_j)^2$ at $x_o=(b/k)(q_i-q_j)$, where b is a damping coefficient produced by charge difference between nearest-neighbor sites (i and j sites) of $\Delta q=(q_i-q_j)$, k is the spring constant of an oxygen atom, (b^2/k) is the strength of electron-phonon interaction, and x_o is a distortion length of a lattice from an equilibrium position. As an example of CDW,[13] when we set two electrons at site i and no electron at the nearest-neighbor site j, the charge ordering (or charge difference) between nearest-neighbor sites is $\Delta q \equiv (q_i-q_j)=(2-0)=2$.

The melting of charge ordering indicates the Peierls MIT where V_{CDW} and x_o approach zero due to $\Delta q \rightarrow 0$. This suggests that the distortion of the structure continuously lessens and finally disappears. Further, the Peierls CDW MIT should exponentially occur with carrier doping or temperature.[13] The sliding of the CDW is for Δq bound by V_{CDW} to tunnel to the nearest-neighbor site. Therefore, Δq is not observed in conduction band by Hall effect measurement. However, since the carriers used for the MIT oscillation are the ones of the conduction band, the tunneling bound charges in V_{CDW} are not used as an electrode. Moreover, the M_2 phase of VO_2 has both charge ordering and a Mott Hubbard insulator; one-half of the V chain pairs but does not twist (this forms charge ordering of CDW) and the other half twists but does not pair (this is an equally spaced V zigzag chain and forms the Mott–Hubbard insulator.).[17,18] Thus, since it has been known that the first-order MIT in VO_2 comes from the equally spaced V chain,[18,30] and that the SPT is continuous,[30] we suggest that the abrupt MIT cannot be explained in terms of the Peierls (CDW) MIT. Note that it can be right that the MIT oscillation is based on the CDW theory for materials following characteristics of CDW such as $K_{0.3}MoO_3$[48] and an organic material.[49,50]

V. CONCLUSION

In conclusion, we have demonstrated sustained electrical oscillations in a simple series circuit comprised of a voltage source, a resistor, and our VO_2 device. These oscillations are the result of the MIT in VO_2. It is shown that these MIT oscillations are attributed to the creation and destruction of a capacitor composed of the semiconducting and metal phases of VO_2. These two phases—coexisting at a nanoscale in VO_2 during the MIT—can be regarded as the dielectric material and electrodes of many nanocapacitors. Since these capacitive components disappear with input heat energy, the MIT oscillation is best explained not in terms of Joule heating inducing a SPT but in terms of hole carriers (or electronic carriers) driving a Mott MIT. Thus, the presence of the MIT oscillation in the VO_2 devices becomes the evidence of the Mott MIT.

Furthermore, the qualitative and quantitative analyses of experimental results suggest that this MIT oscillation, whose frequency can be tuned by active or passive circuit components, can be beneficially applied to fields of power electronics including inverters, high-voltage dc transmission systems, and static synchronous compensators.[58]

ACKNOWLEDGMENTS

This research was supported by the High-Risk High Return project in ETRI, the project on current jump in MKE in Korea, and DOE-BES in America.

[1] N. F. Mott, Rev. Mod. Phys. **40**, 677 (1968).
[2] W. F. Brinkman and T. M. Rice, Phys. Rev. B **2**, 4302 (1970).
[3] H. T. Kim, Physica C **341–348**, 259 (2000).
[4] H. T. Kim, B. J. Kim, Y. W. Lee, B. G. Chae, and S. J. Yun, Physica B **403**, 1434 (2008).
[5] H. T. Kim, B. G. Chae, D. H. Youn, S. L. Maeng, G. Kim, K. Y. Kang, and Y. S. Lim, New J. Phys. **6**, 52 (2004).
[6] C. Ko and S. Ramanathan, Appl. Phys. Lett. **93**, 252101 (2008).
[7] A. Sharoni, APS 2009 March Meeting, Bull. Am. Phys. Soc. **H31–4**, 217 (2009).
[8] M. M. Qazilbash, M. Brehm, B.-G. Chae, P.-C. Ho, G. O. Andreev, B.-J. Kim, S. J. Yun, A. V. Balatsky, M. B. Maple, F. Keilmann, H. T. Kim, and D. N. Basov, Science **318**, 1750 (2007).
[9] D. Ruzmetov, D. Heiman, B. B. Claflin, V. Narayanamurti, and S. Ramanathan, Phys. Rev. B **79**, 153107 (2009).
[10] K. M. Lang, V. Madhavan, J. E. Hoffman, E. W. Hudson, H. Eisaki, S. Uchida, and J. C. Davis, Nature (London) **415**, 412 (2002).
[11] A. Frenzel, M. M. Qazilbash, M. Brehm, B. G. Chae, B. J. Kim, H. T. Kim, A. V. Balatsky, F. Keilmann, and D. N. Basov, Phys. Rev. B **80**, 115115 (2009).
[12] X. Y. Zhang, M. J. Rozenberg, and G. Kotliar, Phys. Rev. Lett. **70**, 1666 (1993).
[13] H. T. Kim, Phys. Rev. B **54**, 90 (1996).
[14] M. Imada, A. Fujimori, and Y. Tokura, Rev. Mod. Phys. **70**, 1039 (1998).
[15] F. J. Morin, Phys. Rev. Lett. **3**, 34 (1959).
[16] J. P. Pouget, H. Launois, J. P. D' Haenens, P. Merenda, and T. M. Rice, Phys. Rev. Lett. **35**, 873 (1975).
[17] M. Marezio, D. B. McWhan, J. P. Remeika, and P. D. Dermier, Phys. Rev. B **5**, 2541 (1972).
[18] T. M. Rice, H. Launois, and J. P. Pouget, Phys. Rev. Lett. **73**, 3042 (1994).
[19] K. W. Lee, H. Kweon, J. Park, and C. E. Lee, Appl. Phys. Lett. **94**, 233111 (2009).
[20] A. Cavalleri, Cs. Tóth, C. W. Siders, J. A. Squier, F. Ráksi, P. Forget, and J. C. Kieffer, Phys. Rev. Lett. **87**, 237401 (2001).
[21] A. Cavalleri, Th. Dekorsy, H. H. W. Chong, J. C. Kieffer, and R. W. Schoenlein, Phys. Rev. B **70**, 161102 (2004).
[22] M. W. Haverkort, Z. Hu, A. Tanaka, W. Reichelt, S. V. Streltsov, M. A. Korotin, V. I. Anisimov, H. H. Hsieh, H. J. Lin, C. T. Chen, D. I. Khomskii, and L. H. Tjeng, Phys. Rev. Lett. **95**, 196404 (2005).
[23] K. Okazaki, S. Sugai, Y. Muraoka, and Z. Hiroi, Phys. Rev. B **73**, 165116 (2006).
[24] S. Biermann, A. Poteryaev, A. I. Lichtenstein, and A. Georges, Phys. Rev. Lett. **94**, 026404 (2005).
[25] H. T. Kim, B. G. Chae, D. H. Youn, G. Kim, K. Y. Kang, S. J. Lee, K. Kim, and Y. S. Lim, Appl. Phys. Lett. **86**, 242101 (2005).
[26] E. Arcangeletti, L. Baldassarre, D. Di Castro, S. Lupi, L. Malavasi, C. Marini, A. Perucchi, and P. Postorino, Phys. Rev. Lett. **98**, 196406 (2007).
[27] J. Sakai and M. Kurish, Phys. Rev. B **78**, 033106 (2008).
[28] C. Chen, R. Wang, L. Shang, and C. Guo, Appl. Phys. Lett. **93**, 171101 (2008).
[29] C. Marini, E. Arcangeletti, D. Di Castro, L. Baldassare, A. Perucchi, S. Lupi, L. Malavasi, L. Boeri, E. Pomjakushina, K. Conder, and P. Postorino, Phys. Rev. B **77**, 235111 (2008).
[30] H. T. Kim, Y. W. Lee, B. J. Kim, B. G. Chae, S. J. Yun, K. Y. Kang, K. J. Han, K. J. Yee, and Y. S. Lim, Phys. Rev. Lett. **97**, 266401 (2006).
[31] B. J. Kim, Y. W. Lee, S. Choi, J. W. Lim, S. J. Yun, H. T. Kim, T. J. Shin, and H. S. Yun, Phys. Rev. B **77**, 235401 (2008).
[32] B. J. Kim, Y. W. Lee, B. G. Chae, S. J. Yun, S. Y. Oh, H. T. Kim, and Y. S. Lim, Appl. Phys. Lett. **90**, 023515 (2007).

[33]J. Wei, Z. Wang, W. Chen, and D. H. Cobden, Nat. Nanotechnol. **4**, 420 (2009).
[34]P. Baum, D. S. Yang, and A. H. Zewail, Science **318**, 788 (2007).
[35]K. L. Holman, T. M. McQueen, A. J. Williams, T. Klimczuk, P. W. Stephens, H. W. Zandbergen, Q. Xu, F. Ronning, and R. J. Cava, Phys. Rev. B **79**, 245114 (2009).
[36]G. Gopalakrishnan, D. Ruzmetov, and S. Ramanathan, J. Mater. Sci. **44**, 5345 (2009).
[37]M. M. Qazilbash, Z. Q. Li, V. Podzorov, M. Brehm, F. Keilmann, B. G. Chae, H. T. Kim, and D. N. Basov, Appl. Phys. Lett. **92**, 241906 (2008).
[38]R. Eguchi, M. Taguchi, M. Matsunami, K. Horiba, K. Yamamoto, Y. Ishida, A. Chainani, Y. Takata, M. Yabashi, D. Miwa, Y. Nishino, K. Tamasaku, T. Ishikawa, Y. Senba, H. Ohashi, Y. Muraoka, Z. Hiroi, and S. Shin, Phys. Rev. B **78**, 075115 (2008).
[39]D. Ruzmetov, S. D. Senanayake, V. Narayanamurti, and S. Ramanathan, Phys. Rev. B **77**, 195442 (2008).
[40]C. Kübler, H. Ehrke, R. Huber, R. Lopez, A. Halabica, R. F. Haglund, Jr., and A. Leitenstorfer, Phys. Rev. Lett. **99**, 116401 (2007).
[41]M. Nakajima, N. Takubo, Z. Hiroi, Y. Ueda, and T. Suemoto, Appl. Phys. Lett. **92**, 011907 (2008).
[42]R. M. Wentzcovitch, W. W. Schulz, and P. B. Allen, Phys. Rev. Lett. **72**, 3389 (1994).
[43]D. Ruzmetov, G. Gopalakrishnan, J. Deng, V. Narayanamurti, and S. Ramanathan, J. Appl. Phys. **106**, 083702 (2009).
[44]When Kim as an author of this paper wrote Ref. 5 on current jump in 2003, he predicted that because the current jump is a change of resistance and not driven by heat, when an appropriate resistance is connected to the MIT device, the MIT oscillation can be generated and be evidence of the Mott MIT. In 2003, since the MIT oscillation was not observed, the research on the MIT oscillation was not inserted into Ref. 5. After then, Kim's researchers tried and discussed to observe the MIT oscillation in VO_2, but they could not succeed. Lee as an author of this paper unexpectedly observed a photo-assisted electrical oscillation and successively found the MIT electrical oscillation. It took over 4 years.
[45]Y. W. Lee, B. J. Kim, J. W. Lim, S. J. Yun, S. Choi, B. G. Chae, G. Kim, and H. T. Kim, Appl. Phys. Lett. **92**, 162903 (2008).
[46]J. Sakai, J. Appl. Phys. **103**, 103708 (2008).
[47]J. B. Gunn, Solid State Commun. **1**, 88 (1963).
[48]A. Maeda, M. Notomi, K. Uchinokura, and S. Tanaka, Phys. Rev. B **36**, 7709 (1987).
[49]F. Sawano, I. Terasaki, H. Mori, T. Mori, M. Watanabe, N. Ikeda, Y. Nogami, and Y. Noda, Nature (London) **437**, 522 (2005).
[50]F. Sawano, T. Suko, T. S. Inada, S. Tasaki, I. Terasaki, H. Mori, T. Mori, Y. Nogami, N. Ikeda, M. Watanabe, and Y. Noda, J. Phys. Soc. Jpn. **78**, 024714 (2009).
[51]B. K. Ridley and T. B. Watkins, Proc. Phys. Soc. **78**, 293 (1961).
[52]N. S. Lee, J. S. Chang, and Y. S. Kwon, J. Electr. Eng. Technol. **1**, 366 (2006).
[53]B. G. Chae, H. T. Kim, S. J. Yun, B. J. Kim, Y. W. Lee, D. H. Youn, and K. Y. Kang, Electrochem. Solid-State Lett. **9**, C12 (2006).
[54]J. Nag and R. F. Haglund, Jr., J. Phys.: Condens. Matter **20**, 264016 (2008).
[55]C. Ko and S. Ramanathan, J. Appl. Phys. **104**, 086105 (2008).
[56]H. S. Choi, J. S. Ahn, J. H. Jung, T. W. Noh, and D. H. Kim, Phys. Rev. B **54**, 4621 (1996).
[57]T. Driscoll, S. Palit, M. M. Qazilbash, M. Brehm, F. Keilmann, B. G. Chae, S. J. Yun, H. T. Kim, S. Y. Cho, N. M. Jokerst, D. R. Smith, and D. N. Basov, Appl. Phys. Lett. **93**, 024101 (2008).
[58]B. Singh and R. Saha, J. Electr. Eng. Technol. **3**, 391 (2008).